Supporting Information

Multifunctional Applications Enabled by Tunable Multi-Emission and Ultra-Broadband Vis-NIR Luminescence via Energy Transfer in Sn^{2+}/Mn^{2+}-Doped Lead-Free Zn- Based Metal Halides

Yongqi Yang [a], Bao Ke [a,], Chengzhi Yang [a], Yang Xue [a], Kaihuang Huang [a], Xintong Lu [b], Bingsuo Zou [a,]**

[a] School of Physical Science and Technology, School of Chemistry and Chemical Engineering, State Key Laboratory of Featured Metal Materials and Life-cycle Safety for Composite Structures, and School of Resources, Environment and Materials, Guangxi University, Nanning 530004, China.

[b] Faculty of Education, The University of Hong Kong, Hong Kong 999077, China

* Address correspondence to E-mail: abner@gxu.edu.cn; zoubs@gxu.edu.cn.

Table S1. Single crystal X-ray diffraction data of $(TPA)_2ZnBr_4$.

Empirical formula	$(TPA)_2ZnBr_4$
Chemical formula	$C_{24}H_{56}Br_4N_2Zn$
Formula weight	757.72
Temperature (K)	296(2)
Crystal system	monoclinic
Space group	C2/c
a (Å)	33.145(5)
b (Å)	14.234(3)
c (Å)	15.081(2)
α (deg)	90
β (deg)	110.207(5)
γ (deg)	90
Volume ($Å^3$)	6677.1(17)
Z	8

Table S2.PL decay parameters of $(TPA)_2ZnBr_4$:Sn^{2+}/Mn^{2+} monitored at 510 nm emission wavelength with different doping concentration of Sn^{2+}.

Sn^{2+} content	τ_1（μs）	τ_2（μs）	τ_{ave}（μs）
0%	0	364.9	361.2
1%	4.58	357.0	356.9
5%	4.68	351.8	351.8
10%	4.75	347.0	346.9
15%	4.81	336.8	336.2
20%	4.85	320.8	320.0
25%	5.54	275.4	270.0

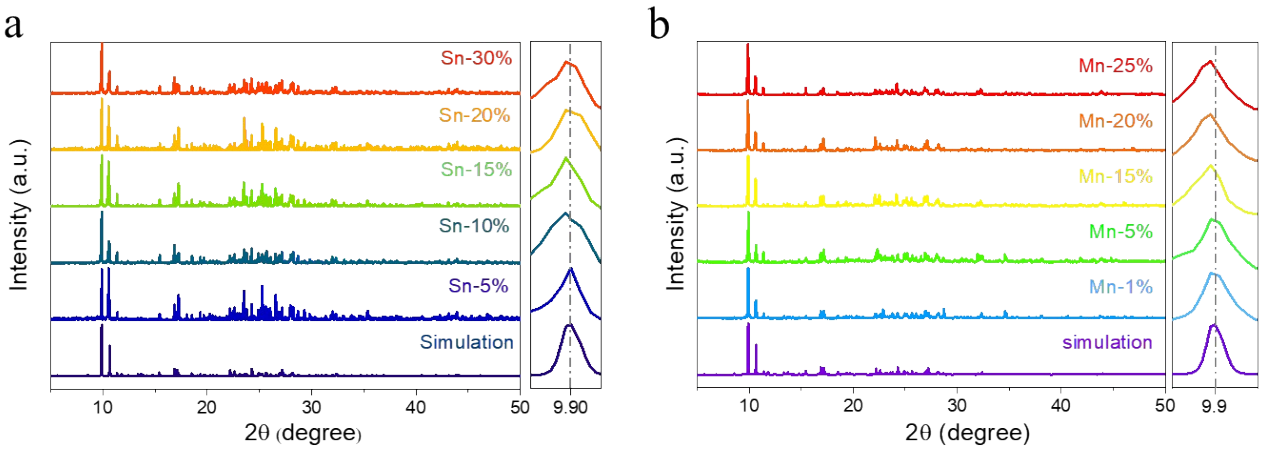

Fig. S1. PXRD patterns of $(TPA)_2ZnBr_4$:*x*%Sn^{2+} **(a)** and $(TPA)_2ZnBr_4$:*x*%Mn^{2+} **(b)**.

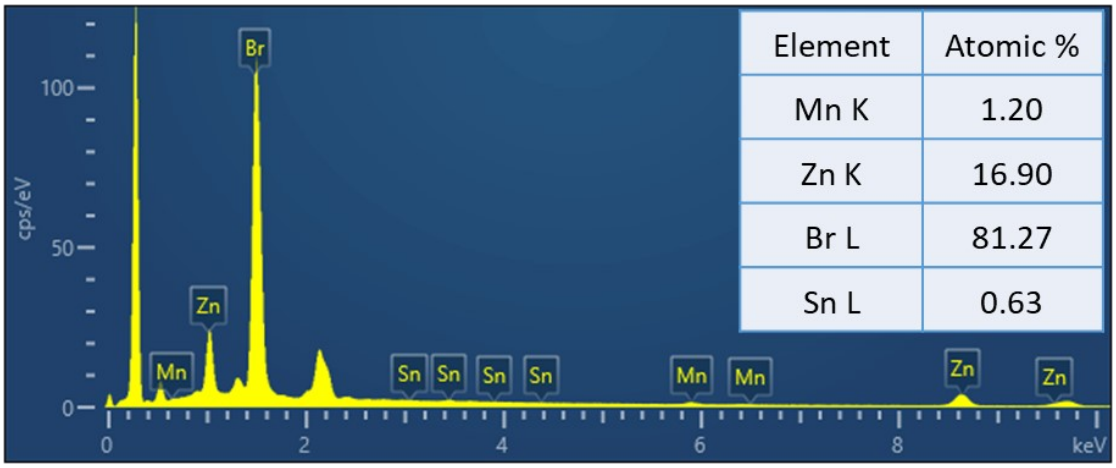

Element	Atomic %
Mn K	1.20
Zn K	16.90
Br L	81.27
Sn L	0.63

Fig. S2. EDS spectrum and element proportion in the $(TPA)_2ZnBr_4$:5%Sn^{2+}/20%Mn^{2+} SCs, the inset table shows the element ratio.

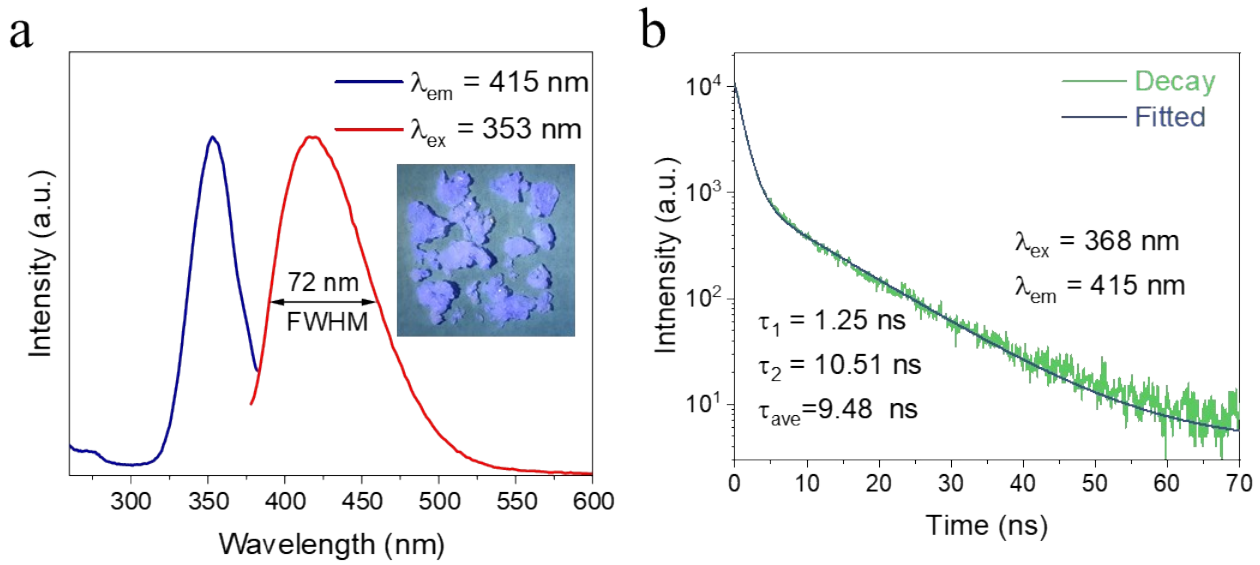

Fig. S3. (a) Normalized PLE and PL spectra of $(TPA)_2ZnBr_4$ (λ_{ex} = 353 nm, λ_{em} = 415 nm). Inset image shows the $(TPA)_2ZnBr_4$ at 365 nm excitation. **(b)** PL decay curves of $(TPA)_2ZnBr_4$ (λ_{ex} = 368 nm, λ_{em} = 415 nm).

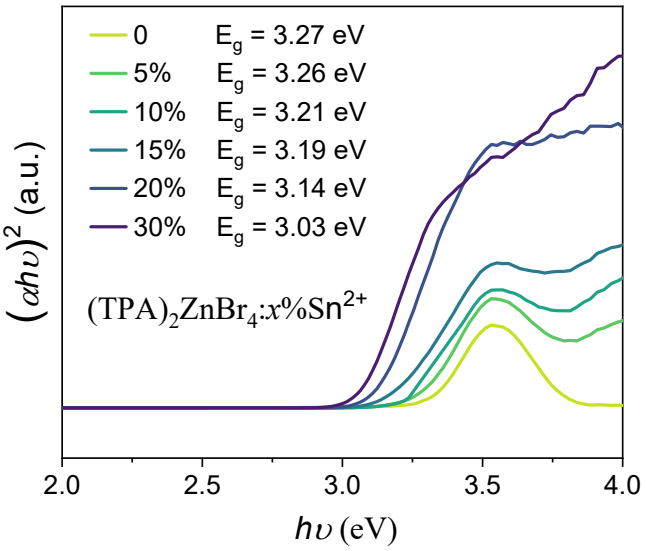

Fig. S4. Tauc plots of the diffuse reflectance spectra of recrystallized $(TPA)_2ZnBr_4$:x%Sn^{2+}. The optical bandgaps (Eg) of the as-prepared samples were calculated by using the Kubelka–Munk theory[1]:

$$[F(R_\infty)h\upsilon]^n = A(h\upsilon - E_g)$$

where R is the reflectance coefficient (%), $h\upsilon$ represents the photon energy, and A represents the absorption constant.

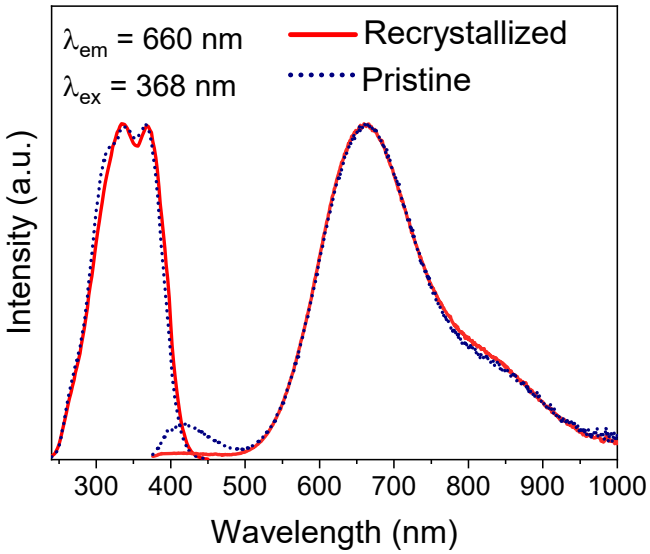

Fig. S5. Normalized PL and PLE spectra of pristine (blue) and recrystallized $(TPA)_2ZnBr_4$:20%Sn^{2+}(red).

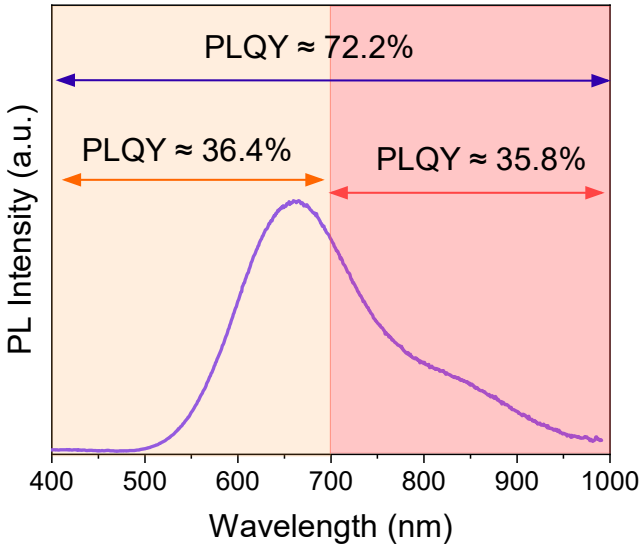

Fig. S6. PL spectra of recrystallized $(TPA)_2ZnBr_4$:20%Sn^{2+} SCs under the excitation of 368 nm. The PLQY of NIR (700–1000 nm) region, and PLQY of the complete broadband spectral region.

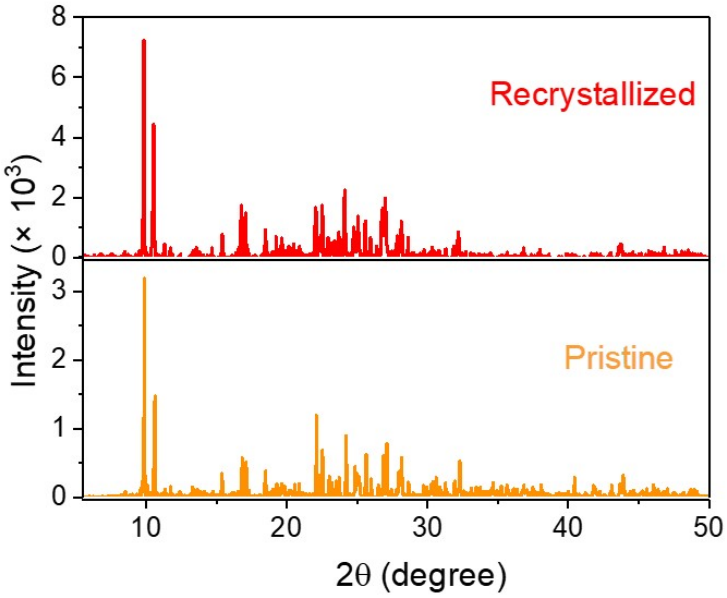

Fig. S7. XRD patterns of the pristine and Recrystallized $(TPA)_2ZnBr_4:Sn^{2+}$.

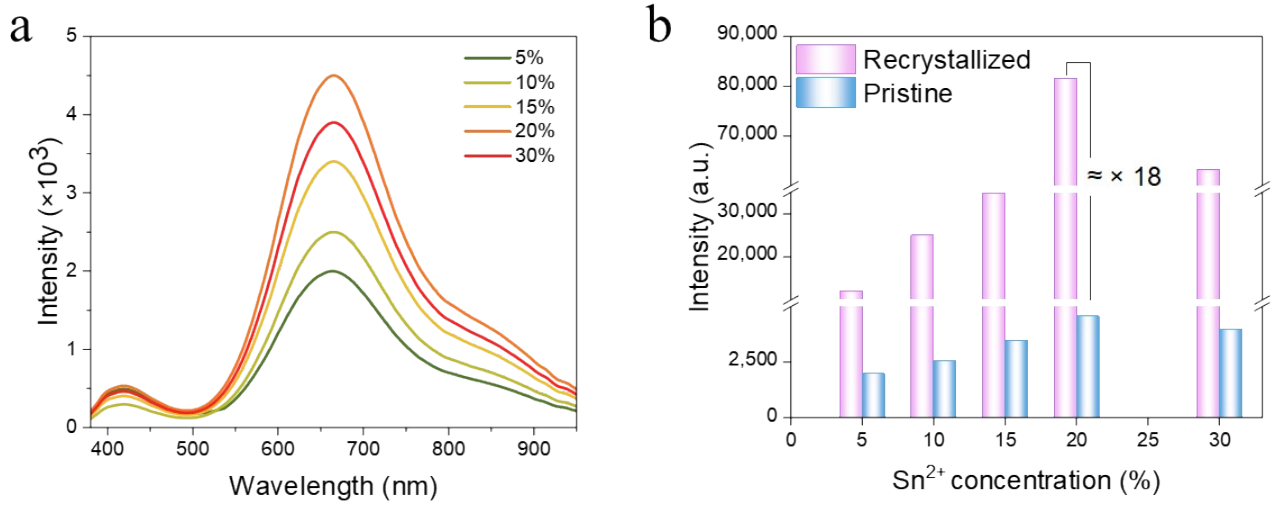

Fig. S8. (a) PL spectra of $(TPA)_2ZnBr_4:x\%Sn^{2+}$ with different Sn^{2+}concentrations (λ_{ex} = 368 nm). **(b)** PL intensity of the pristine and recrystallized $(TPA)_2ZnBr_4$: $x\%Sn^{2+}$ with different Sn^{2+}concentrations.

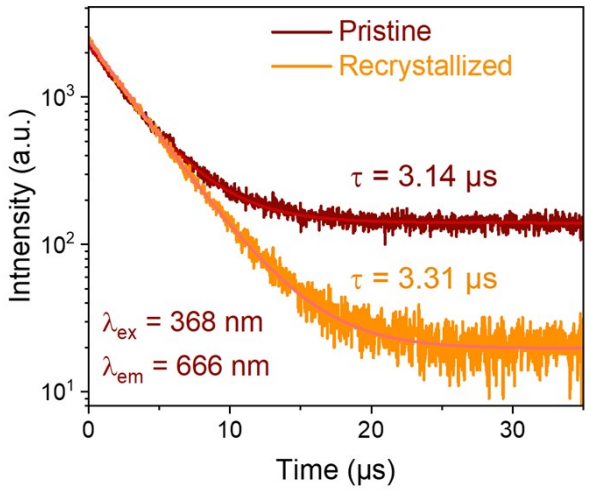

Fig. S9. PL decay curves obtained for the pristine and recrystallized $(TPA)_2ZnBr_4$:20%Sn^{2+}.

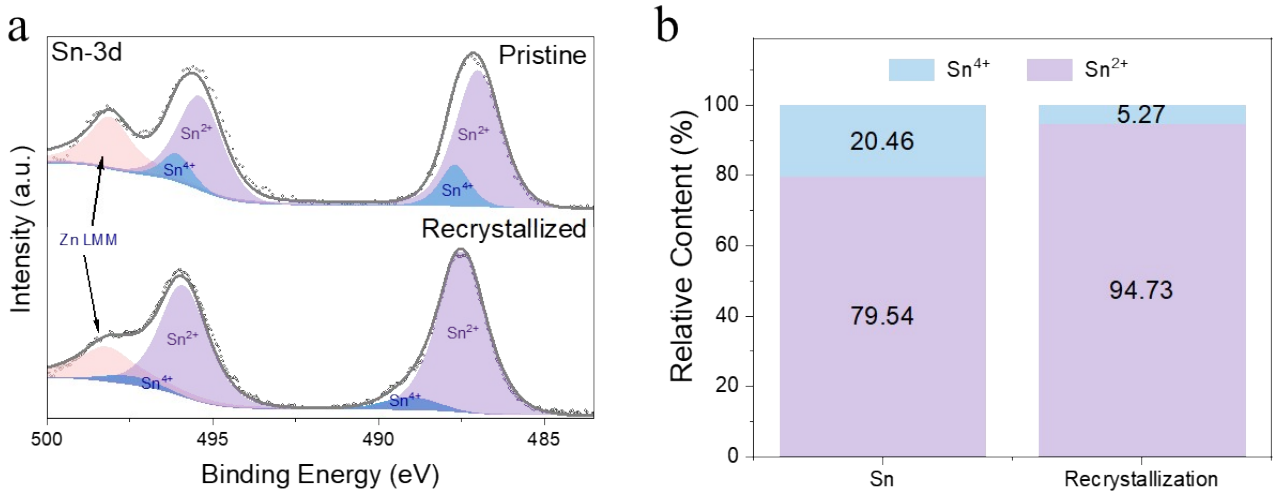

Fig. S10. (a) XPS of Sn 3d spectra. The first peak on the left (pink) is the satellite peak of Zn. **(b)** Proportion of Sn with different valences for the pristine and recrystallized $(TPA)_2ZnBr_4$:20%Sn^{2+}.

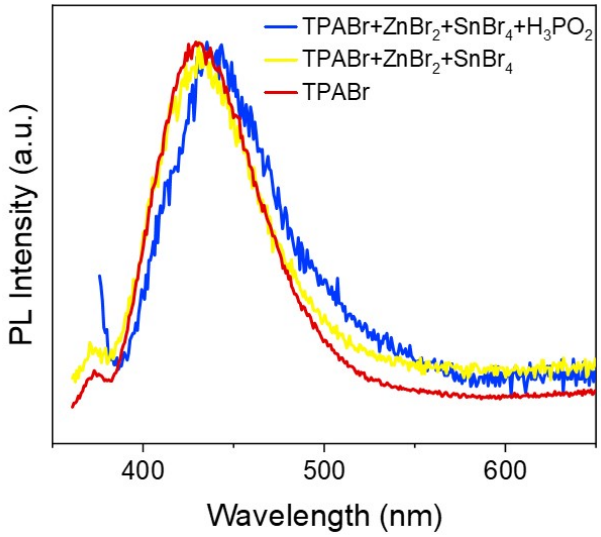

Fig. S11. PL spectra of TPABr and compounds synthesized used $SnBr_4$.

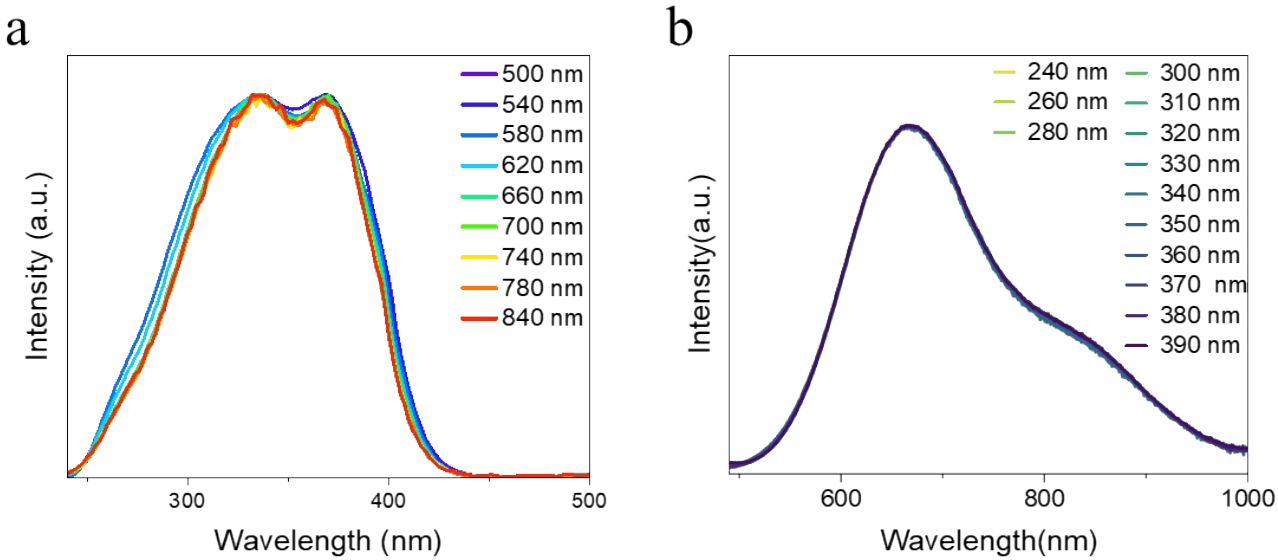

Fig. S12. (a) Emission wavelength-dependent PLE spectra, **(b)** Excitation wavelength-dependent PL spectra of recrystallized $(TPA)_2ZnBr_4$:20%Sn^{2+} SCs at RT.

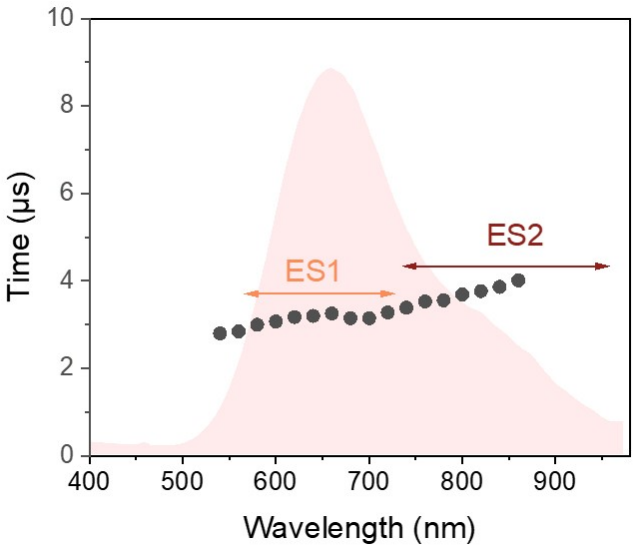

Fig. S13. PL lifetimes at the corresponding wavelengths of recrystallized $(TPA)_2ZnBr_4$:20%Sn^{2+}.

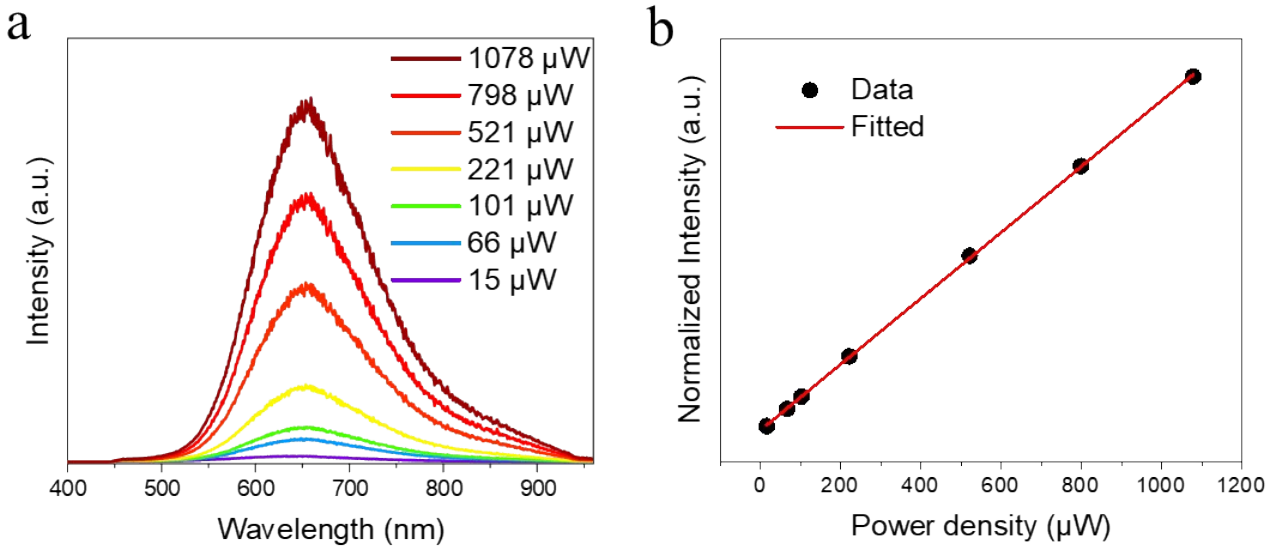

Fig. S14. (a) Excitation power-dependent PL spectra of recrystallized $(TPA)_2ZnBr_4$:20%Sn^{2+} under 405 nm laser excitation. **(b)** Fitting results of PL intensity versus excitation power.

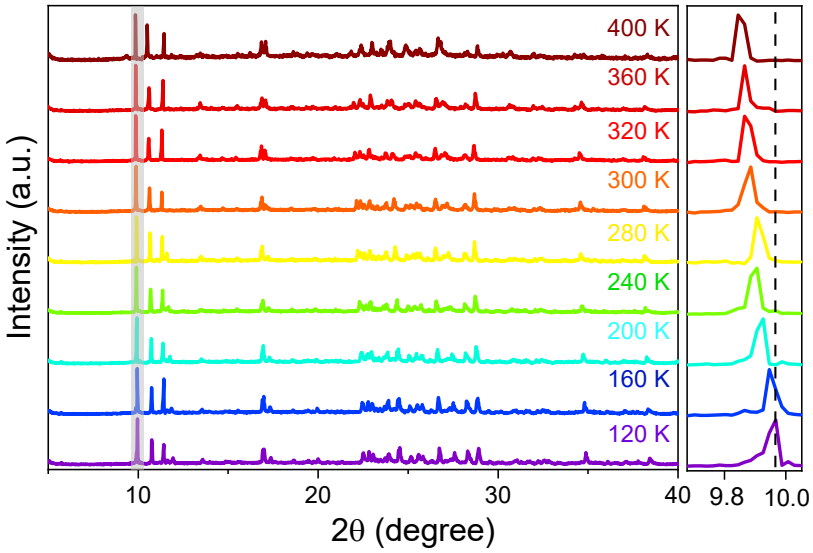

Fig. S15. Temperature-dependent XRD spectra of recrystallized $(TPA)_2ZnBr_4$:20%Sn^{2+}.

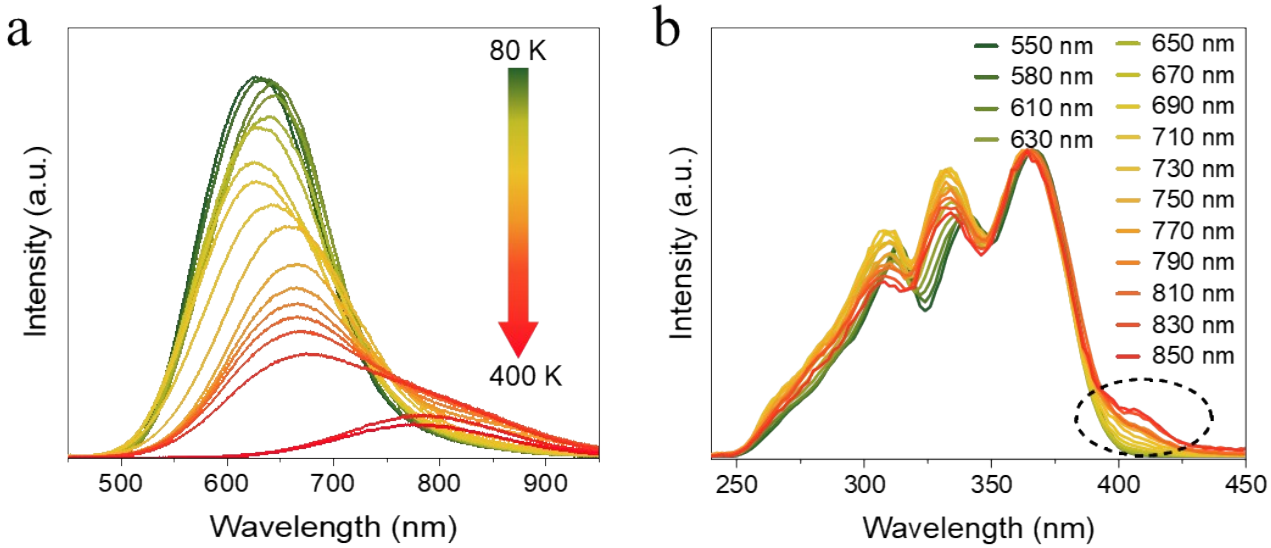

Fig. S16. (a) Temperature dependent PL spectra of recrystallized $(TPA)_2ZnBr_4$:20%Sn^{2+} intervals of 20 K at 368 nm excitation. (b) Emission wavelength-dependent PLE spectra of recrystallized $(TPA)_2ZnBr_4$:20%Sn^{2+} at 80 K.

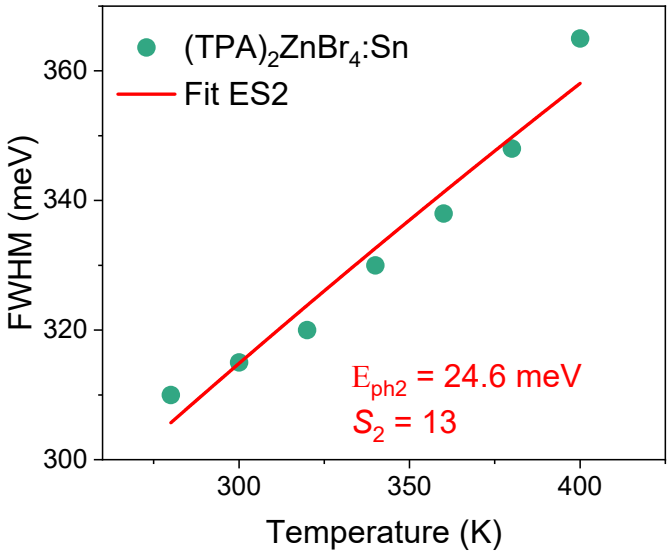

Fig. S17. The fitting result of the function that FWHM of ES2 versus the temperature.

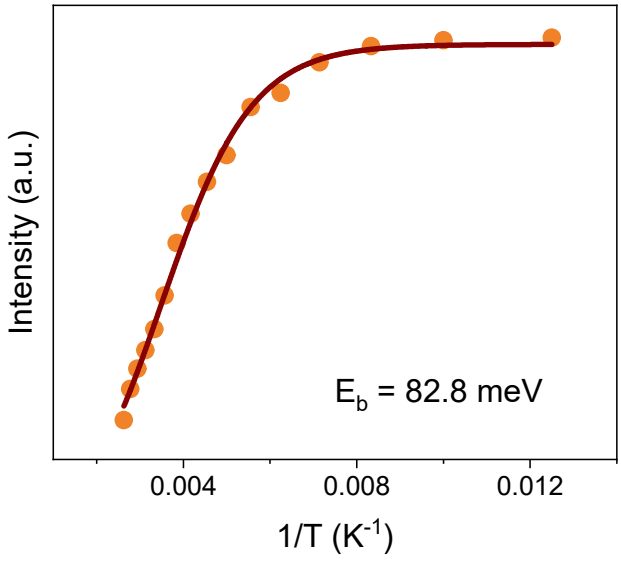

Fig. S18. The fitting result of the function that PL intensity versus the reciprocal of the temperature for $(TPA)_2ZnBr_4$:20%Sn^{2+}.

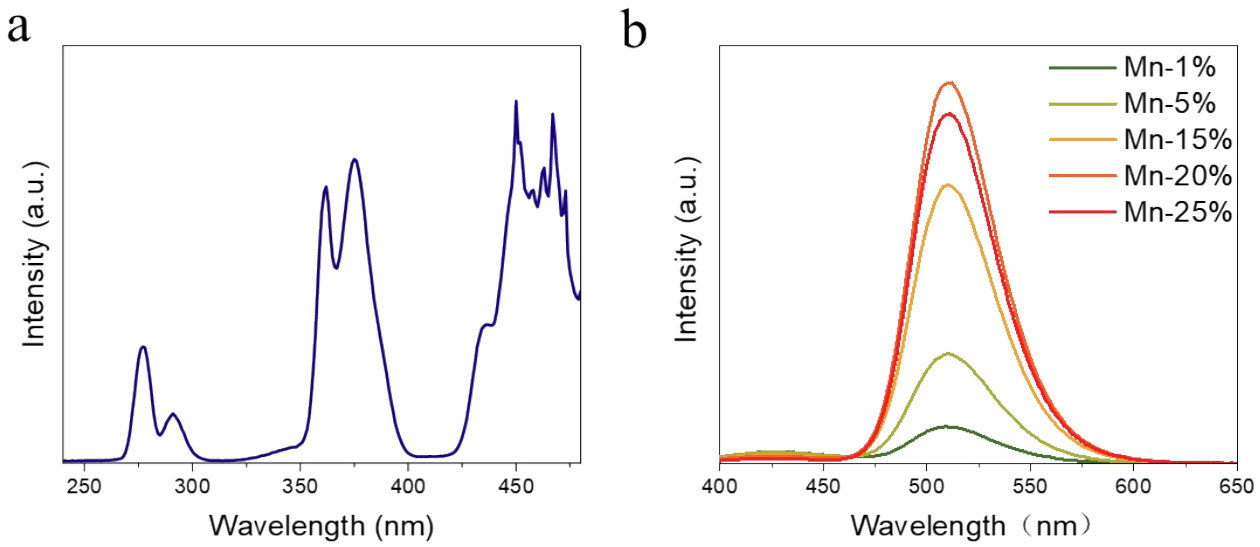

Fig. S19. (a) PLE spectra of $(TPA)_2ZnBr_4:Mn^{2+}$. **(b)** PL spectra (λ_{ex} = 368 nm) of $(TPA)_2ZnBr_4:x\%Mn^{2+}$ with different Mn^{2+}concentrations.

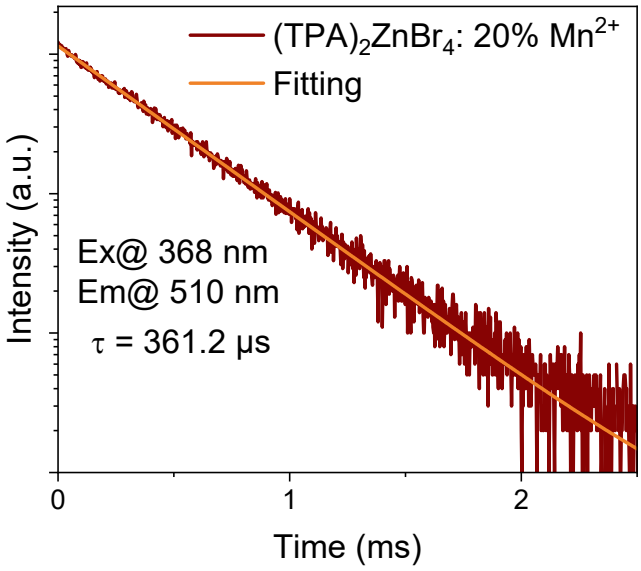

Fig. S20. PL decay curves of $(TPA)_2ZnBr_4:20\%Mn^{2+}$ (λ_{ex} = 368 nm, λ_{em} = 510 nm).

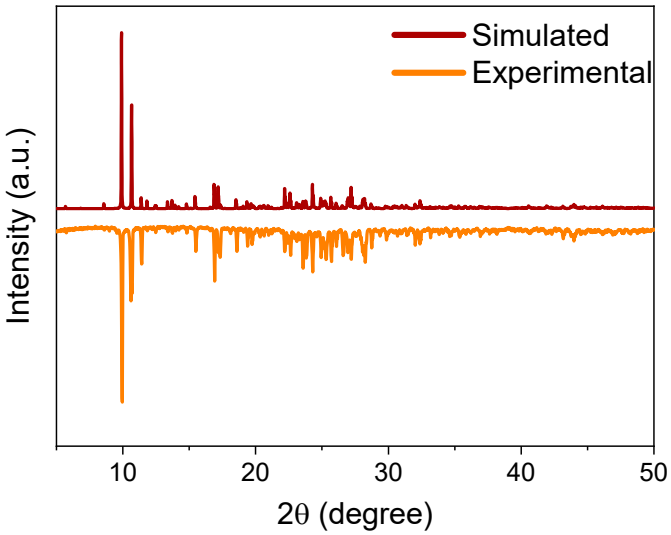

Fig. S21. Experimental and stimulated PXRD patterns of $(TPA)_2ZnBr_4$:5%Sn^{2+}/20%Mn^{2+}.

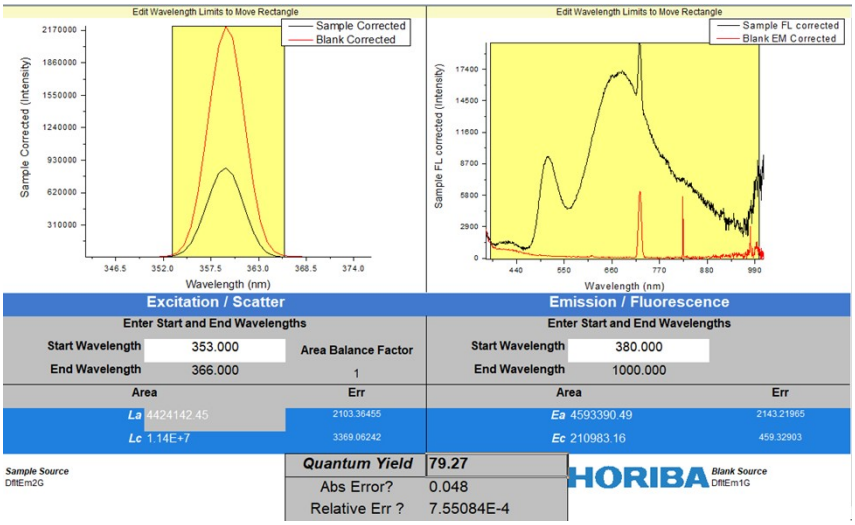

Fig. S22. The maximum PLQY of $(TPA)_2ZnBr_4$: *x*%Sn^{2+}/20%Mn^{2+} SCs.

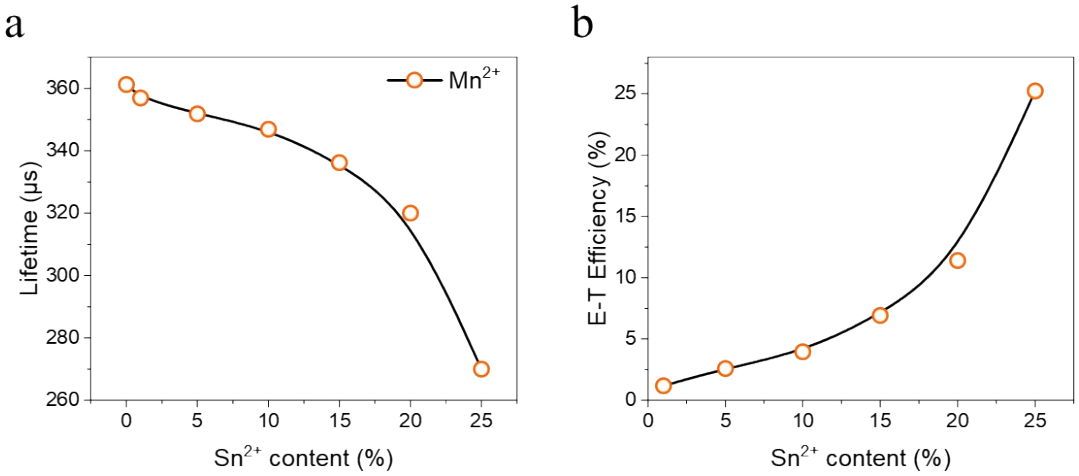

Fig. S23. (a) Lifetime of Mn^{2+} in $(TPA)_2ZnBr_4$:x%Sn^{2+}/20%Mn^{2+} (λ_{ex} = 368 nm, λ_{em} = 510 nm). **(b)** Energy transfer efficiency of $(TPA)_2ZnBr_4$:x%Sn^{2+}/20%Mn^{2+}.[2]

$$\eta_{ET} = 1 - \frac{\tau_x}{\tau_0}$$

where τ_0 is the decay lifetime of STE in $(TPA)_2ZnBr_4$:20% Mn^{2+}, τ_x is the decay lifetime of STE in $(TPA)_2ZnBr_4$:x%Sn^{2+}/20%Mn^{2+} with various Sn^{2+} concentrations.

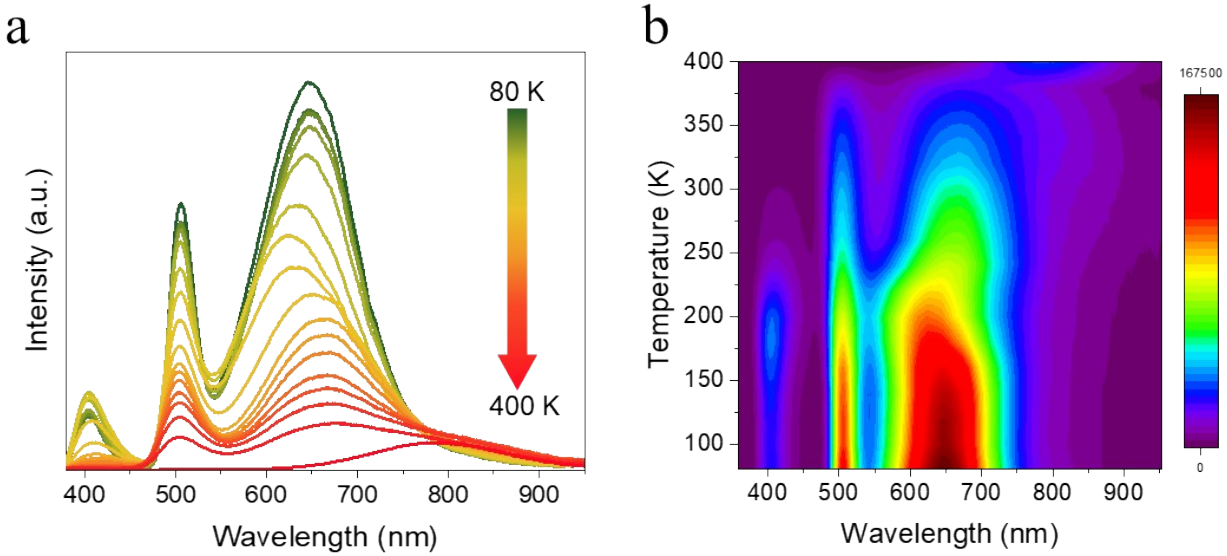

Fig. S24. (a) Temperature-dependent PL spectra of $(TPA)_2ZnBr_4$:10%Sn^{2+}/20%Mn^{2+} excited at 368 nm and corresponding pseudo-color mapping **(b).**

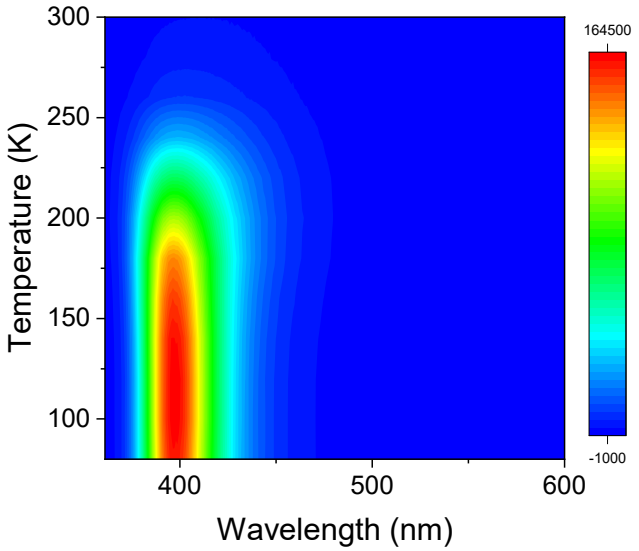

Fig. S25. Temperature-dependent PL spectra of pure $(TPA)_2ZnBr_4$ excited at 368 nm.

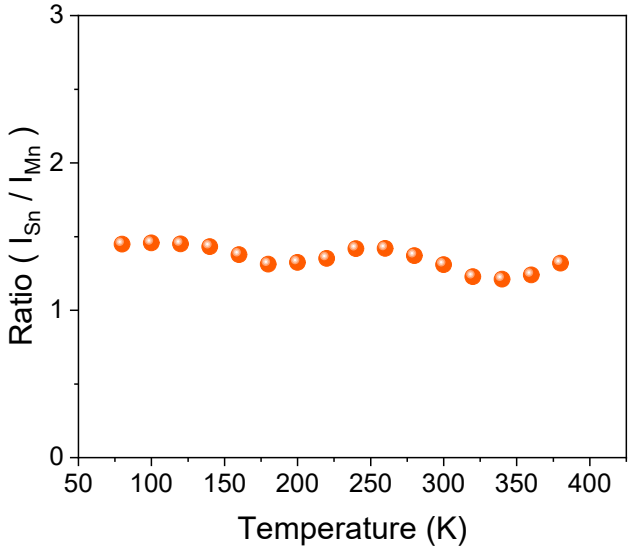

Fig. S26. PL intensity ratio of Sn^{2+} to Mn^{2+} in $(TPA)_2ZnBr_4$:10%Sn^{2+}/20%Mn^{2+} as a function of temperature.

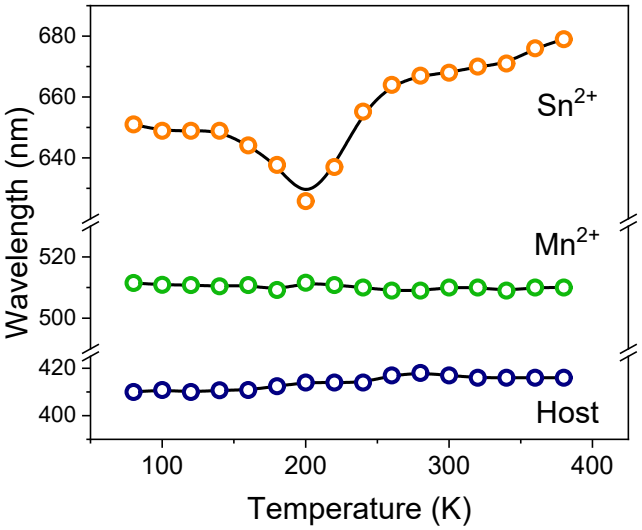

Fig. S27.PL peak position of $(TPA)_2ZnBr_4$:10%Sn^{2+}/20%Mn^{2+}under various temperature.

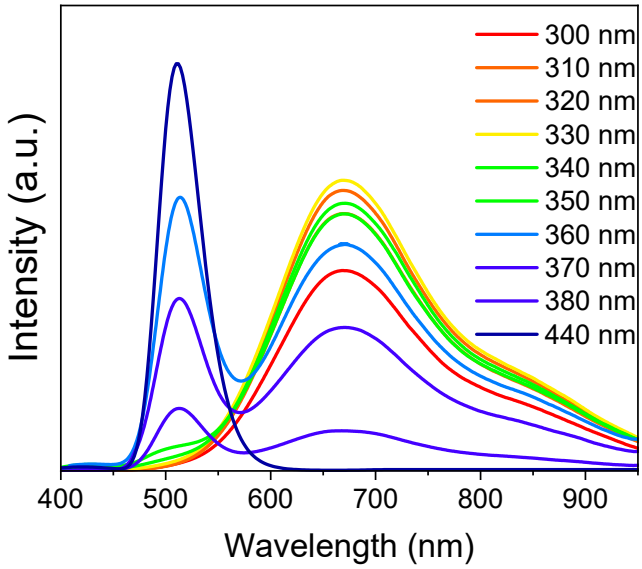

Fig. S28. Excitation wavelength-dependent PL spectra of $(TPA)_2ZnBr_4$:5%Sn^{2+}/20%Mn^{2+}SCs.

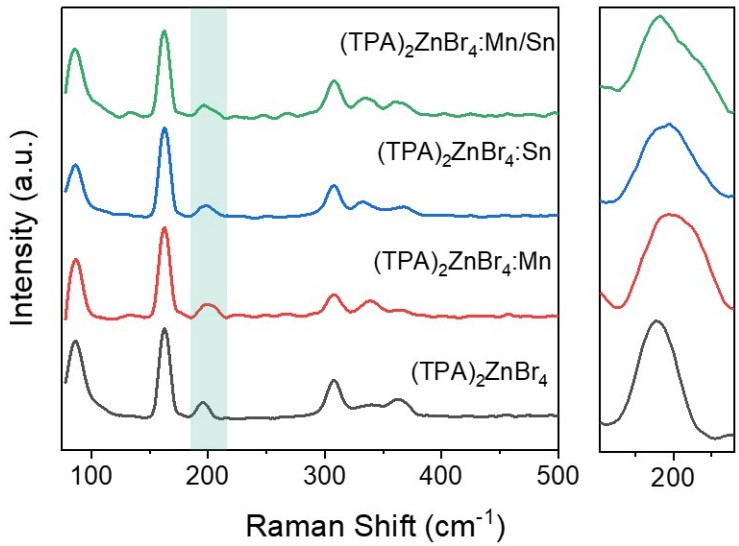

Fig. S29. Raman spectra of pure, Mn^{2+}-doped, Sn^{2+}-doped, and Mn^{2+}/Sn^{2+}-codoped $(TPA)_2ZnBr_4$.

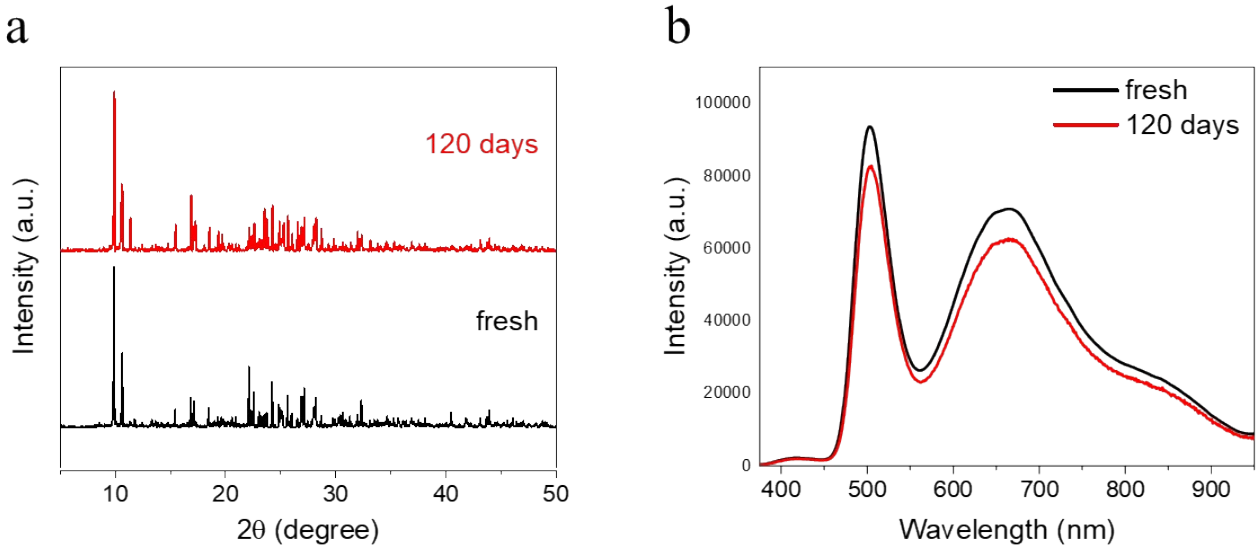

Fig. S30. XRD patterns **(a)** and PL spectra **(b)** of $(TPA)_2ZnBr_4$:5% Sn^{2+}/20%Mn^{2+} stored in atmospheric environment for 120 days.

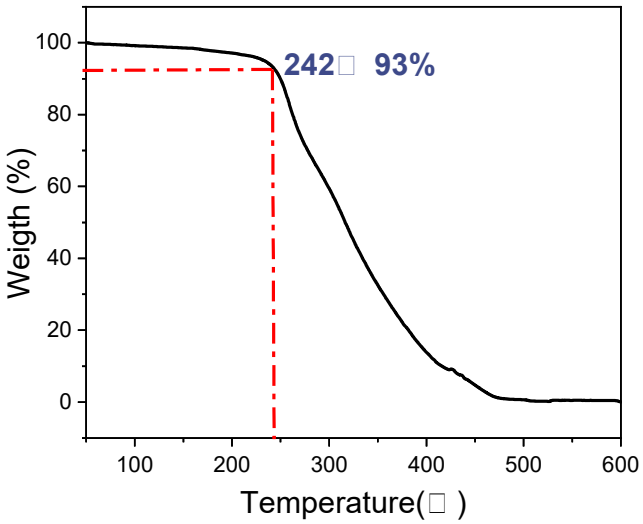

Fig. S31. TG curves of $(TPA)_2ZnBr_4$:5% Sn^{2+}/20%Mn^{2+} powders.

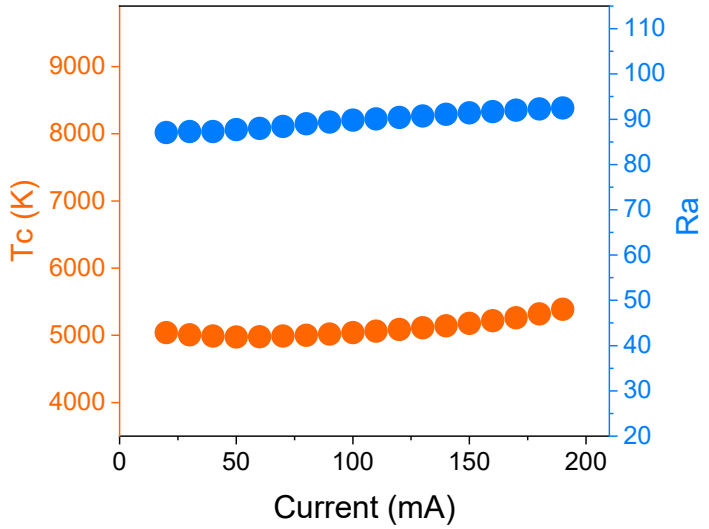

Fig. S32. CRI and CCT stability of the pc-LED device by mixing $(TPA)_2ZnBr_4$:5%Sn^{2+}/20%Mn^{2+} powders with PMMA polymer at various operating currents.

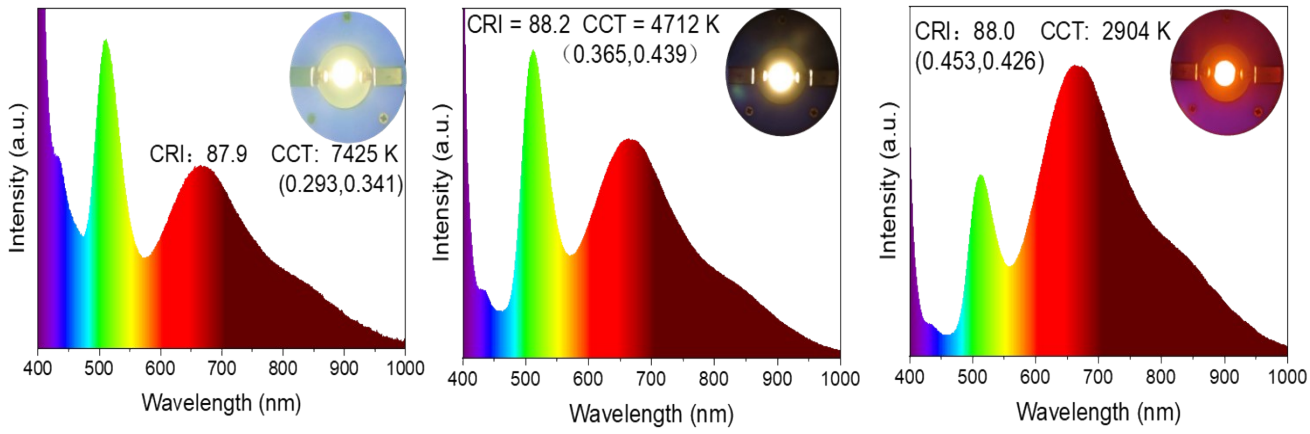

Fig. S33. EL spectra of $(TPA)_2ZnBr_4$:*x*%Sn^{2+}/20%Mn^{2+} pc-LEDs at 60 mA drive current with various Sn^{2+} concentrations, the inset shows the optical photos of the operating pc-LEDs.

REFERENCES

1 R. Zhang, H. Xie, F. Wang, Q. Zhao, L. Meng, Z. Tang, B. Su and H. Liu, *Laser & Photonics Rev*, 2024, **18**, 2400450.

2 L. Cao, X. Jia, W. Gan, C.-G. Ma, J. Zhang, B. Lou and J. Wang, *Adv. Funct. Mater*, 2023, **33**, 2212135.